Photoacoustic emission from Au nanoparticles arrayed on thermal insulation layer

AUTHOR(S):

Namura, Kyoko; Suzuki, Motofumi; Nakajima, Kaoru; Kimura, Kenji

CITATION:

Namura, Kyoko ...[et al]. Photoacoustic emission from Au nanoparticles arrayed on thermal insulation layer. Optics Express 2013, 21(7): 8689-8700

ISSUE DATE:

2013-04

URL:

http://hdl.handle.net/2433/173804

Photoacoustic emission from Au nanoparticles arrayed on thermal insulation layer

Kyoko Namura,[1,2*] Motofumi Suzuki,[1] Kaoru Nakajima,[1] and Kenji Kimura[1]

[1]*Department of Micro Engineering, Kyoto University, Kyoto 606-8501, Japan*
[2]*Research Fellow of the Japan Society for the Promotion of Science*
[*]*namura.kyoko.57r@st.kyoto-u.ac.jp*

Abstract: Efficient photoacoustic emission from Au nanoparticles on a porous SiO_2 layer was investigated experimentally and theoretically. The Au nanoparticle arrays/porous SiO_2/SiO_2/Ag mirror sandwiches, namely, local plasmon resonators, were prepared by dynamic oblique deposition (DOD). Photoacoustic measurements were performed on the local plasmon resonators, whose optical absorption was varied from 0.03 (3%) to 0.95 by varying the thickness of the dielectric SiO_2 layer. The sample with high absorption (0.95) emitted a sound that was eight times stronger than that emitted by graphite (0.94) and three times stronger than that emitted by the sample without the porous SiO_2 layer (0.93). The contribution of the porous SiO_2 layer to the efficient photoacoustic emission was analyzed by means of a numerical method based on a one-dimensional heat transfer model. The result suggested that the low thermal conductivity of the underlying porous layer reduces the amount of heat escaping from the substrate and contributes to the efficient photoacoustic emission from Au nanoparticle arrays. Because both the thermal conductivity and the spatial distribution of the heat generation can be controlled by DOD, the local plasmon resonators produced by DOD are suitable for the spatio-temporal modulation of the local temperature.

OCIS codes: (110.5125) Photoacoustics; (310.4165) Multilayer design.

References and links

1. V. P. Zharov, "Ultrasharp nonlinear photothermal and photoacoustic resonances and holes beyond the spectral limit," Nat. Photon. **5**(2), 110–116 (2011).
2. Y. S. Chen, W. Frey, S. Kim, P. Kruizinga, K. Homan, and S. Emelianov, "Silica-coated gold nanorods as photoacoustic signal nanoamplifiers," Nano Lett. **11**(2), 348–354 (2011).
3. H. Tian, D. Xie, Y. Yang, T. L. Ren, Y. X. Lin, Y. Chen, Y. F. Wang, C. J. Zhou, P. G. Peng, L. G. Wang, and L. T. Liu, "Flexible, ultrathin, and transparent sound-emitting devices using silver nanowires film," Appl. Phys. Lett. **99** 253507 (2011).
4. Y. Hou, J.-S. Kim, M. O'Donnel, and L. J. Guo, "Optical generation of high frequency ultrasound using two-dimensional gold nanostructure," Appl. Phys. Lett. **89,** 093901 (2006).
5. V. P. Zharov, T. V. Malinsky, and R. C. Kurten, "Photoacoustic tweezers with a pulsed laser: theory and experiments," J. Phys. D: Appl. Phys. **38** 2662–2674 (2005).
6. D. Braun and A. Libchaber, "Trapping of DNA by thermophoretic depletion and convection," Phys. Rev. Lett. **89**(18) 188103 (2002).

#183695 - $15.00 USD Received 17 Jan 2013; revised 1 Mar 2013; accepted 4 Mar 2013; published 2 Apr 2013

7. L. H. Thamdrup, N. B. Larsen, and A. Kristensen, "Light-induced local heating for thermophoretic manipulation of DNA in polymer micro- and nanochannels," Nano Lett. **10**(3) 826–832 (2010).
8. B. Auguié and W. L. Barnes, "Collective resonances in gold nanoparticle arrays," Phys. Rev. Lett. **101,** 143902(4) (2008).
9. J. Parsons, E. Hendry, C. P. Burrows, B. Auguié, J. R. Sambles, and W. L. Barnes, "Localized surface-plasmon resonances in periodic nondiffracting metallic nanoparticle and nanohole arrays," Phys. Rev. B **79,** 073412(7) (2009).
10. M. Suzuki, Y. Imai, H. Tokunaga, K. Nakajima, K. Kimura, T. Fukuoka, and Y. Mori, "Tailoring coupling of light to local plasmons by using Ag nanorods/structured dielectric/mirror sandwiches," J. Nanophotonics **3,** 031502 (2009).
11. M. Suzuki, K. Nakajima, K. Kimura, T. Fukuoka, and Y. Mori, "Au nanorod arrays tailored for surface-enhanced Raman spectroscopy," Anal. Sci. **23**(7), 829–833 (2007).
12. A. Leitner, Z. Zhao, H. Brunner, F. R. Aussenegg, and A. Wokaun, "Optical properties of a metal island film close to a smooth metal surface," Appl. Opt. **32**(1), 102–110 (1993).
13. K. Namura, M. Suzuki, K. Nakajima, and K. Kimura, "Heat-generating property of a local plasmon resonator under illumination," Opt. Lett. **36,** 3533–3535 (2011).
14. H. Shinoda, T. Nakajima, K. Ueno, and N. Koshida, "Thermally induced ultrasonic emission from porous silicon," Nature **400,** 853–855 (1999).
15. A. Rosencwaig and A. Gersho, "Theory of the photoacoustic effect with solids," J. Appl. Phys. **48**(1), 64–69 (1976).
16. C. M. Pitsillides, E. K. Joe, X. Wei, R. R. Anderson, and C. P. Lin, "Selective cell targeting with light-absorbing microparticles and nanoparticles," Biophys. J. **84**, 4023–4032 (2003).
17. Y. A. Avetisyan, A. N. Yakunin, and V. V. Tuchin, "Thermal energy transfer by plasmon-resonant composite nanoparticles at pulse laser irradiation," Appl. Opt. **51**(10), C88–C94 (2012).
18. National Astronomical Observatory of Japan, *Chronological Science Tables* (Tokyo: Maruzen, 1993).
19. M. Suzuki and Y. Taga, "Numerical study of the effective surface area of obliquely deposited thin films," J. Appl. Phys. **90**(11), 5599–5605 (2001).

1. Introduction

Photoacoustic emission from noble metal nanoparticles has gained much attention owing to their potential applications in the field of sound-emitting devices, photoacoustic imaging, and ultrasonic trapping with standing-waves in the high frequency range ($>$ 1 MHz) [1–5], and manipulation of fluid or particles by convection flow and thermophoresis in the low frequency range ($<$ 20 Hz) [5–7]. Although the frequency of the photoacoustic emission for these applications is varied over a very wide range, the fundamental mechanism of the acoustic emission is essentially identical. The light absorbed by the nanoparticles is converted into heat that spontaneously causes thermal expansion of the surrounding gas. This expanding gas layer acts as an acoustic piston and produces acoustic pressure. Thus, understanding and controlling of the coupling between photons and phonons are of great importance in all of the practical applications of the photoacoustic emission.

There are two general methods for generating the photoacoustic emission from noble metal nanoparticles. The ultrasonic generation from the colloidal gold solutions irradiated by pulsed or chopped light has been reported in several papers and has shown good potential for photoacoustic imaging [1–3]. Although such solutions are suitable for generating strong photoacoustic emission from nanoclusters within a beam spot, it is difficult to define the location of the sound-emitting sources. On the other hand, two-dimensional Au nanoparticle arrays, which are often fabricated by the electron-beam lithography of Au thin films on a glass or Si substrate, generate photoacoustic emission from a well-defined location [4]. This allows us to achieve coherent photoacoustic emission from spatially arranged Au nanoparticle arrays. However, two-dimensional Au nanoparticle arrays absorb only a few tens of percent of the incident light even at the wavelength of the local plasma resonance [8, 9].

Recently, we demonstrated the self-assembly of Au nanoparticle array/structured dielectric layer/Ag mirror sandwiches, i.e., a local plasmon resonator, using a dynamic oblique deposition (DOD) technique [10]. The structured dielectric layer consists of two layers, which are named

#183695 - $15.00 USD Received 17 Jan 2013; revised 1 Mar 2013; accepted 4 Mar 2013; published 2 Apr 2013

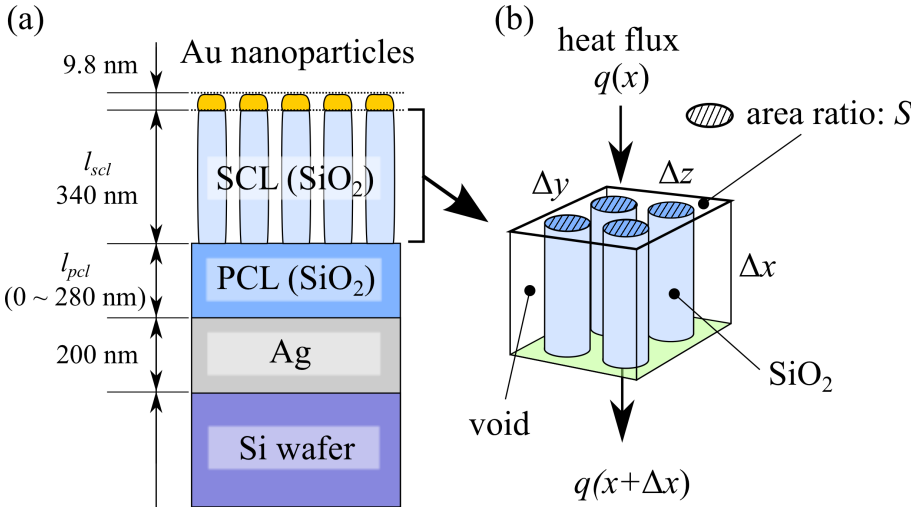

Fig. 1. (a) Schematic drawing of side view of local plasmon resonator with Au nanoparticle array/SCL/PCL/Ag mirror structure. (b) Volume element of the SCL with cylindrical columns. The filling factor, S, is equal to the area ratio.

Table 1. The list of samples, where α represents the deposition angle.

	With SCL		Without SCL	
	thickness (nm)	α (°)	thickness (nm)	α (°)
Au nanoparticle arrays	9.8	83.4	9.8	83.4
SCL (SiO_2)	340	78.6	–	–
PCL (SiO_2)	0–280	0	310–500	0
Ag mirror	200	0	200	0

the shape control layer (SCL) and the phase control layer (PCL). The SCL is a porous SiO_2 columnar layer and controls the shape of the Au nanoparticles. The PCL is a SiO_2 plane layer and controls the optical path length. Because of strong interference, local plasmon resonators can be used to alter the optical absorption value of the two-dimensional Au nanoparticle arrays in the range of $\sim$ 0 to 0.99 by varying the thickness of the dielectric layer [11, 12]. In our previous study, we reported the efficient photothermal conversion of local plasmon resonators [13]. For these local plasmon resonators, we expect highly amplified photoacoustic emission from the Au nanoparticle arrays owing to the thermal insulating effect of the porous SiO_2 layer, since the efficiency of the thermally induced acoustic emission from a thin metal film is known to be largely dependent on the thermal properties of the underlying layer [14]. In this work, we present a systematic study of the photoacoustic emission from local plasmon resonators and clarify their structural advantages in the low frequency range ($<$ 100 kHz), of which notion is also useful in the treatment of high frequency photoacoustic emission.

2. Experiments

We prepared local plasmon resonators with Au nanoparticles/SCL/PCL/Ag mirror structure (Fig. 1) by using DOD. The local plasmon resonators were prepared by electron beam evaporation under a pressure of 5×10^{-4} Pa with a deposition rate of 0.2–0.3 nm/s. First, a smooth Ag

#183695 - $15.00 USD Received 17 Jan 2013; revised 1 Mar 2013; accepted 4 Mar 2013; published 2 Apr 2013

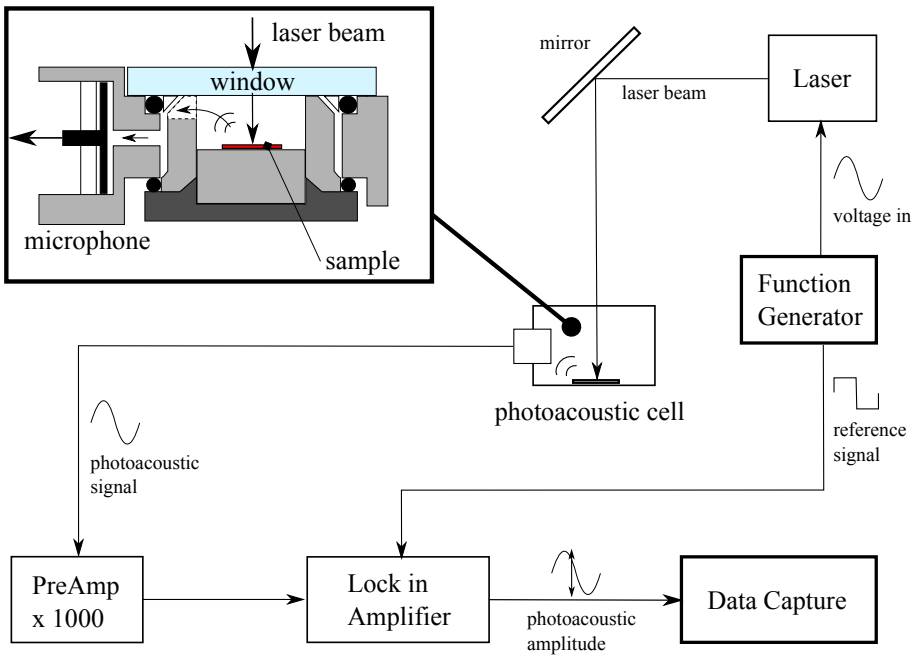

Fig. 2. Experimental setup for photoacoustic measurements.

layer with 200 nm thickness was deposited on a Si wafer. Onto this Ag mirror surface, a phase control layer (PCL) of SiO_2 was deposited with the vapor normally incident to the surface. The PCL thickness, l_{pcl}, was varied from 0 nm to 280 nm as listed in Table 1 in order to obtain samples with a wide range of optical absorption. This series of different SiO_2 thicknesses were realized on a single substrate by moving a shutter incrementally across the sample during SiO_2 deposition. On the PCL, a shape control layer (SCL) of SiO_2 was prepared; this layer was evaporated until it reached a thickness of 340 nm. During the deposition of the SCL, the deposition angle (measured as an angle from the normal) was fixed at 78.6° and the substrate was rotated continuously and rapidly. An Au nanoparticle layer with 9.8 nm thickness was deposited at a deposition angle of 83.4° onto the SCL. In order to investigate the contribution of the porous SCL layer to the photoacoustic amplitude, we also prepared local plasmon resonators without an SCL. In the case of the preparation of samples without an SCL, the step of SCL deposition was skipped and the PCL thickness was varied from 310 nm to 500 nm. The optical reflection measurements at an angle of incidence of 2° were carried out using a single-beam spectrophotometer in the wavelength range of 300 nm $< \lambda <$ 1700 nm. Since the optical transmittance and scattering of our samples are negligibly small, their optical absorption A is evaluated as $A = 1 - R$, where R is the optical reflectance.

The photoacoustic measurements were performed using a photoacoustic cell (10.0 mm in diameter and 3.5 mm height, MTEC Model 300) on the local plasmon resonators with and without SCL, bulk graphite, and Ag thin film. The experimental setup used for the measurements is depicted in Fig. 2. We loaded the sample, which was cut into a small piece of 4 mm × 4 mm × 0.5 mm size, onto the photoacoustic cell filled with air. Then, the chip was irradiated with a laser (wavelength 785 nm), whose intensity was modulated sinusoidally, from the surface normal. The photoacoustic signal detected by a microphone was measured with a lock-in amplifier and recorded as a function of the laser modulation frequency over the range from 0.1

#183695 - $15.00 USD Received 17 Jan 2013; revised 1 Mar 2013; accepted 4 Mar 2013; published 2 Apr 2013

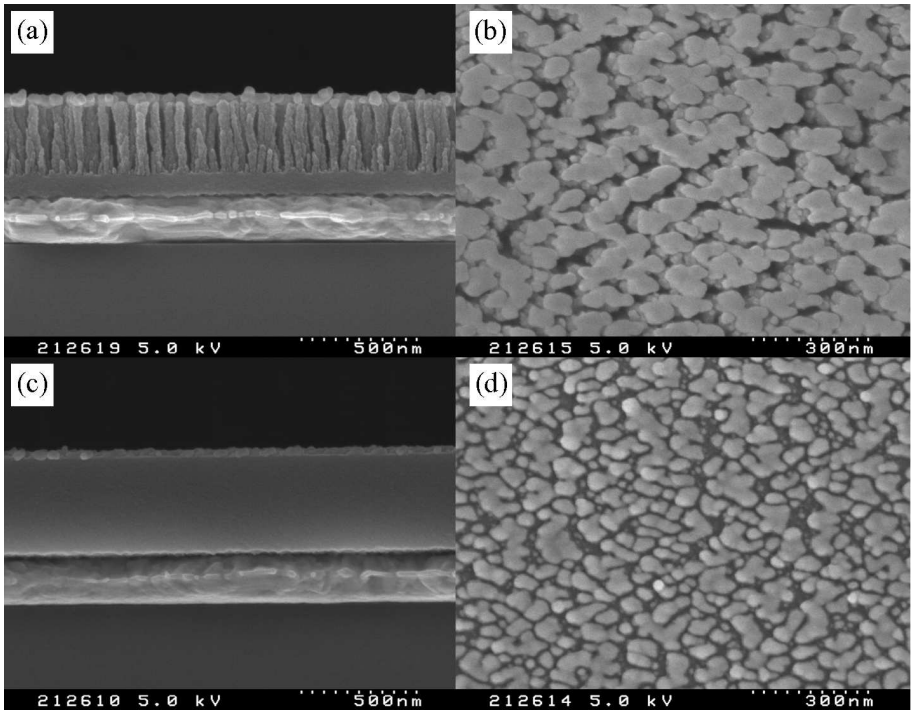

Fig. 3. SEM images of (a) the cross section and (b) the surface morphology of the local plasmon resonator with an Au nanoparticle array/SCL/PCL/Ag mirror structure. (c) and (d) SEM images of the sample with an Au nanoparticle array/PCL/Ag mirror structure.

kHz to 100 kHz.

3. Results and discussion

3.1. Morphology and optical properties

Figure 3 show typical SEM images of the prepared local plasmon resonators with and without SCL. From the SEM image of the cross section of each sample (Figs. 3(a) and 3(c)), it is clear that the multilayered structures of Au nanoparticles/SiO_2 dielectric layer/Ag mirror are realized by DOD. In the case of the Au nanoparticle arrays, the local plasmon resonator with an SCL has a porous SiO_2 layer (340 nm thick), whereas the sample without the SCL has no pores in the dielectric layer. However, the thicknesses of the Au nanoparticle layers are equally small regardless of the existence of the SCL. In addition, as shown in Figs. 3(b) and 3(d), granular morphology is realized in the samples with and without SCL. Although the structures in Fig. 3(b) are slightly larger than those in Fig. 3(d), heat transfer from Au nanoparticles to air may not drastically differ dipending on the existence of the SCL.

Figure 4 shows the optical absorption spectra of the local plasmon resonators with and without an SCL. The optical absorption of the local plasmon resonators changes periodically as a function of the photon energy, and the absorption peaks change drastically with the PCL thickness. These spectral properties originate from the interference [10, 12, 13] and can be understood by multilayered homogeneous layers at least around NIR or longer wavelength region because dimensions of the nanostructures in the layers are much smaller than that of the wavelength. In those wavelength region, the Au nanoparticles layer is treated as an effective medium

#183695 - $15.00 USD Received 17 Jan 2013; revised 1 Mar 2013; accepted 4 Mar 2013; published 2 Apr 2013

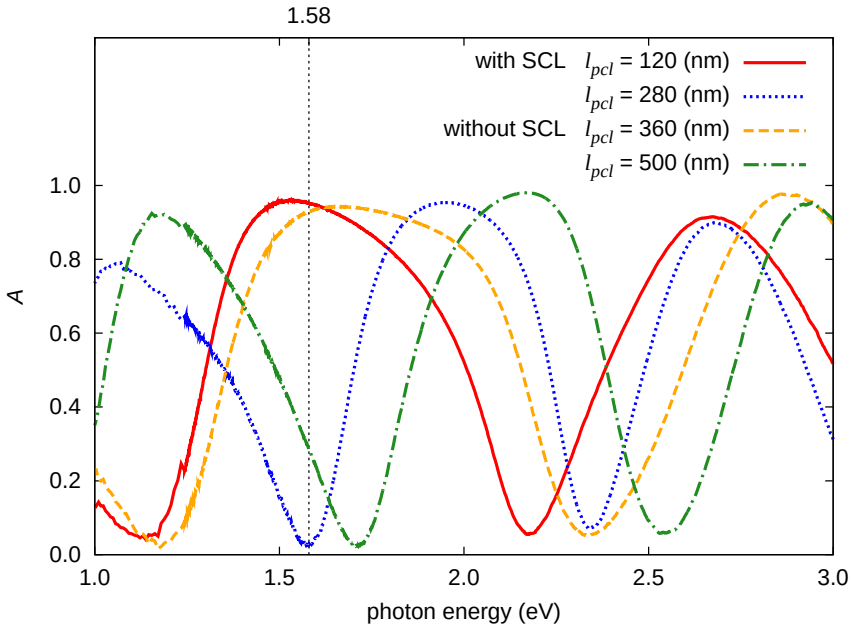

Fig. 4. Optical absorption spectra of the local plasmon resonators with an SCL ($l_{pcl} = 120$ nm and 280 nm thickness) and without an SCL ($l_{pcl} = 360$ nm and 500 nm thickness)

which includes the material with a constant permittivity and Au nanoparticles of which dielectric function is represented by the Drude model. The SCL is also treated as a homogeneous medium of which permittivity is 1.20–1.25. The PCL and the Ag mirror are of course uniform SiO_2 and Ag layers. The details have been reported in the previous paper [10] for Ag nanoparticles/dielectric spacer/Ag mirror structures, which is essentially identical with the structures in the present study. In the Fig. 4, the coupling of the light to the local plasmons in Au nanoparticles is successfully modified, regardless of the existence of the SCL. At the wavelength of 785 nm (1.58 eV) in the photoacoustic measurements, the optical absorption, *A*, of the prepared local plasmon resonators with the SCL changes from 0.03 to 0.95, while that of the samples without the SCL changes from 0.28 to 0.93.

3.2. Photoacoustic properties

We performed photoacoustic measurements on the local plasmon resonators in order to evaluate the contribution of their optical absorption and of the porous SCL to the photoacoustic amplitude. Figure 5 shows the typical photoacoustic spectra of the local plasmon resonators with an SCL (A = 0.95 and 0.03) and without an SCL (A = 0.93), in addition to the photoacoustic spectra of graphite (A = 0.95) and Ag (A = 0.01). In the spectra, many distinct peaks are observed. Since the peak positions are independent of the samples, the peaks originate from the acoustic resonance in the photoacoustic cell. However, as indicated in Fig. 2, the shape of the photoacoustic cell is too complex to analyze its resonance modes. Thus, we focus our attention on the relative amplitudes of the obtained spectra.

In Fig. 5, the photoacoustic amplitude, *P*, of the local plasmon resonator with an SCL having high optical absorption (A = 0.95) is approximately eight times larger than that of graphite (A = 0.94) and three times larger than that of the sample without an SCL (A = 0.93). On the other hand, the signal from the sample with an SCL having low absorption (A = 0.03) has the same

#183695 - $15.00 USD Received 17 Jan 2013; revised 1 Mar 2013; accepted 4 Mar 2013; published 2 Apr 2013

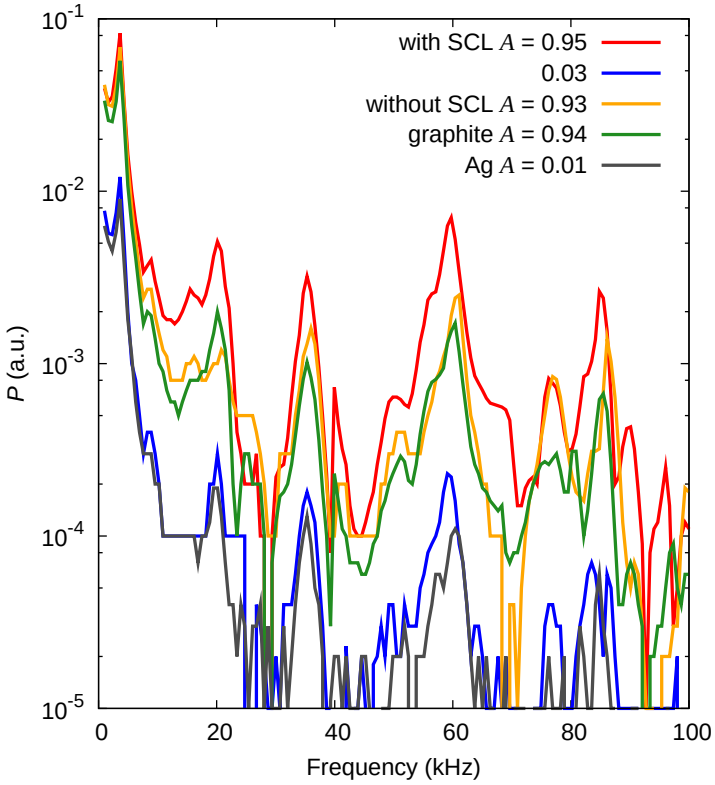

Fig. 5. Photoacoustic spectra of the local plasmon resonators with an SCL (A = 0.95 and 0.03) and without an SCL (A = 0.93), in addition to those of graphite (A = 0.94) and Ag (A = 0.01).

order of magnitude as that from the high reflective Ag thin film (A = 0.01). These results suggest that the local plasmon resonators with an SCL can realize efficient photoacoustic emission and spatial modulation by the tuning of the thickness of the PCL.

In order to understand the effect of nanostructures on the photoacoustic properties, we focused our attention on the properties of two series of samples with and without an SCL. For both series of samples, we successfully realized the similar ranges of $310 < l_{pcl} + l_{scl} < 510$ nm and $0.25 < A < 0.95$, while the amount of deposited Au was kept constant at 9.8 nm. Figure 6 show some of the photoacoustic spectra of those local plasmon resonators, with an SCL (Fig. 6(a)) and without an SCL (Fig. 6(b)), as a function of the laser modulation frequency. The signal amplitude of the samples with the SCL varies significantly depending on the sample, while that of the samples without the SCL varies only slightly. For quantitative comparison, we listed photoacoustic amplitude at the laser modulation frequency of 60 kHz, optical absorption, l_{scl}, and l_{pcl} of all samples in Table 2. The value of P seems to show a monotonic increase with an increasing A. However, it is worth noting that the photoacoustic amplitude of the Au nanoparticle array depends not only on A but also on the thickness of the underlying dielectric layer [15]. Since the heat generated from the Au nanoparticles is expected to be proportional to their optical absorption [13], we plotted the ratio of P at the laser modulation frequency of 60 kHz to A, for each sample, as a function of the dielectric thickness, $l_{pcl} + l_{scl}$ (Fig. 7). The value of P/A is almost independent of the thickness of the dielectric layer. This supports the result that

#183695 - $15.00 USD Received 17 Jan 2013; revised 1 Mar 2013; accepted 4 Mar 2013; published 2 Apr 2013

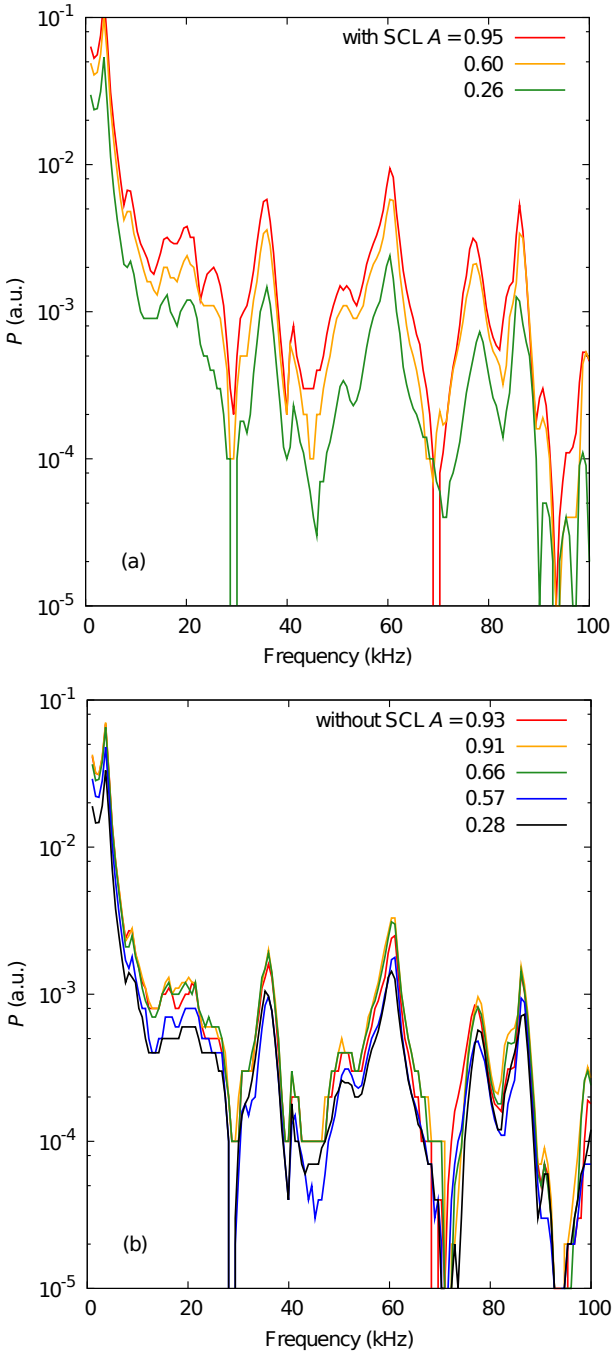

Fig. 6. Typical photoacoustic spectra of local plasmon resonators, (a) with an SCL and (b) without an SCL, for various optical absorption values.

#183695 - $15.00 USD Received 17 Jan 2013; revised 1 Mar 2013; accepted 4 Mar 2013; published 2 Apr 2013

Table 2. Properties of the local plasmon resonators with and without an SCL.

	P at 60 kHz (10^{-2} a.u.)	A	l_{scl} (nm)	l_{pcl} (nm)
With SCL	1.07	0.95	340	132
	0.92	0.92	340	110
	1.18	0.94	340	88
	1.07	0.95	340	88
	0.94	0.95	340	82
	0.96	0.93	340	71
	1.20	0.88	340	66
	0.97	0.94	340	66
	0.83	0.82	340	44
	0.58	0.60	340	22
	0.24	0.26	340	0
Without SCL	0.24	0.93	0	360
	0.33	0.91	0	410
	0.31	0.66	0	460
	0.17	0.57	0	505
	0.14	0.28	0	310

P is essentially proportional to A. On the other hand, P/A is highly sensitive to the existence of the porous SCL, and the local plasmon resonators with an SCL are capable of producing photoacoustic signals with an approximately threefold higher amplitude than those without an SCL.

3.3. *Heat transfer model*

In order to clarify the contribution of the porosity and the thickness of the dielectric layer to the photoacoustic amplitude, we investigated the thermally induced acoustic emission from the local plasmon resonator with an SCL, on the basis of a one-dimensional heat transfer model, as depicted in Fig. 8. We assume that the system of the local plasmon resonator and the photoacoustic cell is composed of the Si, PCL, SCL, and gas (air) layers and that their thicknesses are l_{si}, l_{pcl}, l_{scl}, and l_g, respectively. Although the actual local plasmon resonators have the Ag mirror layer (200 nm) on the Si wafer, its thickness is significantly smaller than the thermal diffusion length of Ag and is negligible because of the uniformity of temperature inside the layer. In addition, we assume the Au nanoparticle layer at the top of the sample as a heat source whose thickness is negligibly small, because the thickness of the Au nanoparticle layer is significantly smaller than those of the other layers and the incident light is absorbed and converted into heat by the nanoparticle layer [10, 13]. This assumption is justified because the temperature inside Au nanoparticles is expected to be uniform when excitation laser intensity is modulated at lower than 100 kHz, although there are several reports on pulsed laser excitation which causes inhomogeneous temperature distribution inside nanoparticles [16, 17]. We define the sample surface to be at $x = 0$, and hence, the heat applied by the photothermal conversion is assumed to be

$$q(x,t) = AQ_0(1+\cos\omega t)\,\delta(x), \tag{1}$$

where t is the time (s), Q_0 is the power density of the incident light (W/m^2), and ω is the laser modulation frequency (s^{-1}).

Assuming that there is no convection in the cell, the heat diffusion equation for each layer is

#183695 - $15.00 USD Received 17 Jan 2013; revised 1 Mar 2013; accepted 4 Mar 2013; published 2 Apr 2013

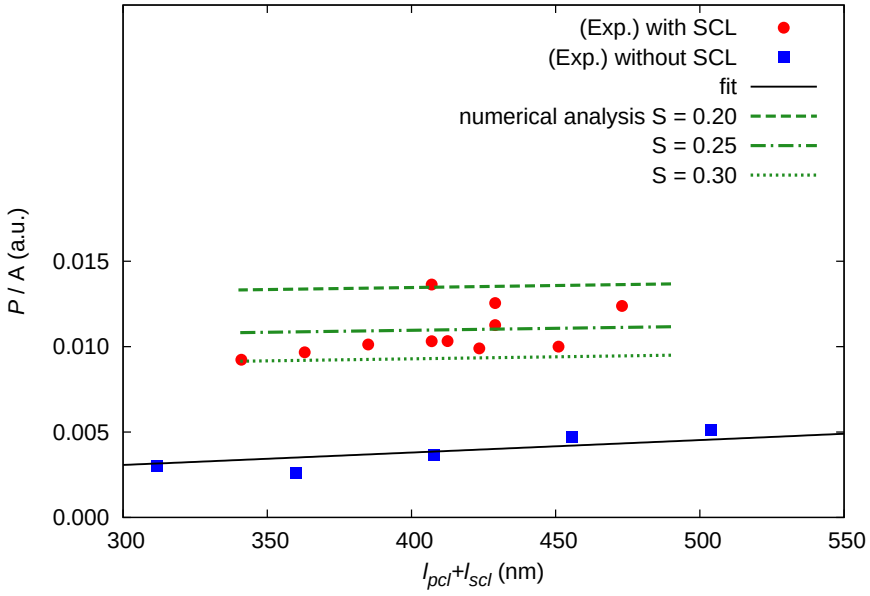

Fig. 7. Photoacoustic amplitude, P, over optical absorption, A, as a function of the thickness of the dielectric layer, $l_{pcl} + l_{scl}$, at the laser modulation frequency of 60 kHz. The solid line is the fitting result of the theoretical solution for the samples without an SCL. The dashed lines are the results of the numerical analysis for the samples with an SCL, for the filling factors, $S = 0.20$, 0.25, and 0.30.

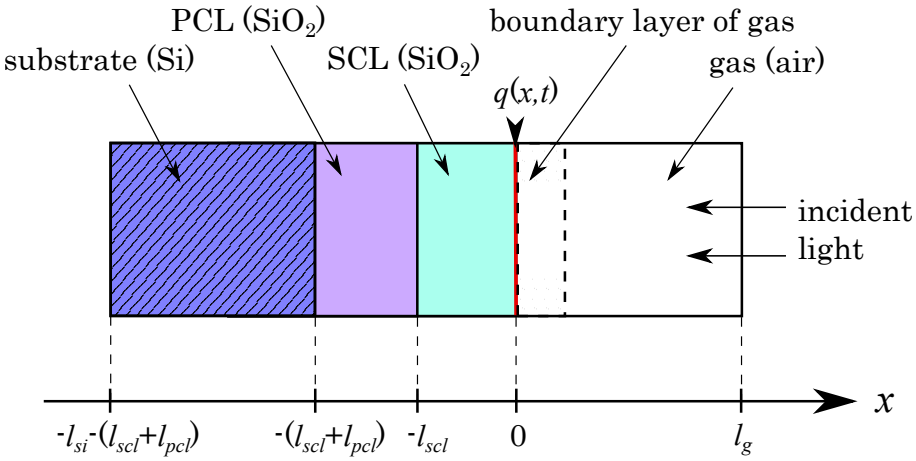

Fig. 8. Schematic diagram of heat transfer model and the coordinate configuration.

#183695 - $15.00 USD Received 17 Jan 2013; revised 1 Mar 2013; accepted 4 Mar 2013; published 2 Apr 2013

written as

$$\frac{\partial u_i(x,t)}{\partial t} = a_i \frac{\partial^2 u_i(x,t)}{\partial x^2}. \tag{2}$$

Here, u_i is the temperature (K) and a_i is the thermal diffusivity (m^2/s) defined by $a_i = \kappa_i/\rho_i C_i$, where κ_i, ρ_i, and C_i are the thermal conductivity (W/m s), density (kg/m^3), and specific heat (J/kg K) of the material i, respectively. The subscript i becomes si, scl, pcl, and g for the Si wafer, SCL, PCL, and gas (air), respectively. Equation (2) is solved under the boundary conditions that the temperature and heat-flux are continuous at interfaces. In addition, we assume that the temperature at the cell walls $x = l_g$ and $x = -l_{si} - (l_{scl} + l_{pcl})$ is the ambient temperature, T_0.

The general solution for $u(0,t) \equiv u_{scl}(0,t) = u_g(0,t)$ can be written as

$$u(0,t) = U_{dc} + U_{ac}\cos(\omega t + \phi), \tag{3}$$

where U_{dc} and U_{ac} are complex-valued constants and ϕ is a real-valued constant for the phase factor. This periodic temperature change of the sample surface simultaneously causes expansion and contraction within a thin boundary layer of the gas next to the surface and produces acoustic pressure signals [15]. According to the derivation of Rosencwaig and Gersho [15], the photoacoustic amplitude can be written as

$$P = F\frac{|U_{ac}|}{|U_{dc}|}, \tag{4}$$

where F is a real-valued constant that can be determined by the shape of the photoacoustic cell and the property of the surrounding gas. In other words, F is essentially independent of the sample properties.

In order to obtain the value of F for our measurement system, we focus on the photoacoustic properties of the samples without an SCL that have a simple structure. For such samples, $l_{scl} = 0$ and the analytical solution for Eq. (3) is written as

$$U_{dc} = T_0 + \frac{AQ_0 l_g\left(\kappa_{pcl}l_{si} + \kappa_{si}l_{pcl}\right)}{\kappa_{pcl}\kappa_{si}l_g + \kappa_g\left(\kappa_{pcl}l_{si} + \kappa_{si}l_{pcl}\right)}, \tag{5}$$

$$U_{ac} = \frac{AQ_0}{\kappa_{pcl}\sigma_{pcl}}\frac{(1-b)\exp(-\sigma_{pcl}l_{pcl}) + (1+b)\exp(\sigma_{pcl}l_{pcl})}{(1+c)(1+b)\exp(\sigma_{pcl}l_{pcl}) - (1-c)(1-b)\exp(-\sigma_{pcl}l_{pcl})}, \tag{6}$$

where

$$\sigma_i = (1+j)\left(\frac{\omega}{2a_i}\right)^{1/2}, b = \frac{\kappa_{si}\sigma_{si}}{\kappa_{pcl}\sigma_{pcl}}, c = \frac{\kappa_g\sigma_g}{\kappa_{pcl}\sigma_{pcl}}. \tag{7}$$

The real part of Eq. (6) represents the actual physical temperature variation. In the experiment, $T_0 = 2.9\times10^2$ (K), $A < 1$, $Q_0 = 4.0\times10^4$ (W/m^2), $\kappa_{si} = 1.5\times10^2$ (W/m K), $\kappa_{pcl} = 1.4$ (W/m K), $\kappa_g = 2.4\times10^{-2}$ (W/m K), $l_{si} = 0.5\times10^3$ (μm), and $l_g = 3.5\times10^3$ (μm) [18]. Therefore, the second term on the right-hand side of Eq. (5) is smaller than 1.4 (K). Consequently, we can assume $|U_{dc}| \simeq T_0 = 290$ (K). In Eqs. (6) and (7), $a_{pcl} = 6.2\times10^{-7}$ (m^2/s), $a_{si} = 9.0\times10^{-5}$ (m^2/s), and $a_g = 1.9\times10^{-5}$ (m^2/s). By substituting Eqs. (5)–(7) into Eq. (4), we obtain the photoacoustic amplitude of the local plasmon resonator without an SCL. Since the $|U_{dc}|$ in Eq. (5) is almost constant and $|\sigma_{pcl}l_{pcl}|$ in the Eq. (6) is small ($< 5\times10^{-7}$ ($s^{1/2}$)), the P is estimated to be almost independent of the dielectric thickness. The solid line shown in Fig. 7 shows the results of fitting the analytical solution to the experimental data, where F is the fitting parameter. We obtain the prefactor $F = 76\pm5$ from the fitting. The calculated data agrees well with the experimental data, which is almost independent of the dielectric thickness.

#183695 - $15.00 USD Received 17 Jan 2013; revised 1 Mar 2013; accepted 4 Mar 2013; published 2 Apr 2013

The value of F evaluated for the samples without an SCL was utilized to discuss the photoacoustic emission from the samples with an SCL. Since the samples with an SCL have many layers, it is difficult to derive an analytical solution for $|U_{ac}/U_{dc}|$ in Eq. (4). Thus, we performed a numerical calculation for the heat transfer model. Before performing the calculation, we needed to determine the SCL thermal diffusivity, a_{scl}, and the thermal conductivity, κ_{scl}. When we consider the one-dimensional energy balance of the volume element depicted in Fig. 1(b), κ_{scl} determines the heat flux in the direction normal to the interfaces, induced by the temperature gradient. As can be seen in the SEM image of the local plasmon resonator with an SCL (Fig. 3(a)), the SCL is composed of cylindrical SiO_2 columns growing along the surface normal. Therefore, the filling factor, S, is equal to the area fraction of SiO_2, as depicted in Fig. 1(b). The magnitudes of κ_{scl} and $\rho_{scl}C_{scl}$ are S times as large as those in the case of SiO_2. Thus, the thermal diffusivity of the SCL, $a_{scl} = \kappa_{scl}/\rho_{scl}C_{scl}$, is equal to that of SiO_2.

The results of the numerical analysis of the photoacoustic amplitude for $S = 0.20$, 0.25, and 0.30 are shown in Fig. 7. The calculation agrees with the experimental results when S is in the range of 0.25–0.30. From the SEM images shown in Fig. 3 and in the previous paper [19], the filling factor of the SCL deposited at the deposition angle of $\sim 80^\circ$ is estimated to be in the range of 0.3–0.4. This value is close to that determined in the present numerical analysis, even though the photoacoustic amplitude, P/A, exhibits high sensitivity to the filling factor, S. This result suggests that the photoacoustic amplitude is strongly dependent on the porosity of the SCL layer, which determines the thermal conductivity of the layer under the Au nanoparticles. By reducing the thermal conductivity of the underlying layer, the heat flux from the Au nanoparticles to the substrate is decreased and that to the air is increased. Accordingly, the local temperature of the air is efficiently modulated and substantial photoacoustic emission is realized. Consequently, the low conductivity of the layer that contributes to the efficient photoacoustic emission is easily achieved by the DOD technique. Further improvement of the photoacoustic amplitude can be achieved by reducing the filling factor of the SCL layer or by utilizing materials with low thermal conductivity to form the layer.

4. Conclusion

We performed photoacoustic measurements on local plasmon resonators with Au nanoparticle arrays/SCL (porous SiO_2 layer)/PCL/Ag mirror structures achieved by DOD. The photoacoustic amplitude of the local plasmon resonator with high absorption (A = 0.95) is eight times larger than that of graphite (A = 0.94) and three times larger than that of the sample without a porous SCL layer (A = 0.93). In addition, the signal from the local plasmon resonator with low absorption (A = 0.03) has the same order of magnitude as that from the highly reflective Ag thin film (A = 0.01). In order to verify the contribution of the porous SCL layer to the efficient photoacoustic emission, theoretical and numerical analyses based on the one-dimensional heat transfer model were performed. The results suggest that the low thermal conductivity of the porous SCL layer, which is easily formed by DOD, contributes to the reduction of the amount of heat escaping to the substrate and to the efficient photoacoustic emission from Au nanoparticle arrays. Overall, a very promising feature of the local plasmon resonators with a porous SCL is their spatio-temporal controllability of heat generation. They are suitable for use in nanoheaters, which can be used for microfluidic control using photoacoustic generation and thermophoresis, as well as in sound-emitting devices.

Acknowledgments

We are grateful to Sadamu Kinoshita from Kyoto University for assisting us with the SEM observations. This work was supported by JSPS KAKENHI Grant Number 21656058, 24·2362 and the Japanese-Taiwanese Cooperative Programme on ”Nano Device.”

#183695 - $15.00 USD Received 17 Jan 2013; revised 1 Mar 2013; accepted 4 Mar 2013; published 2 Apr 2013